Molecular Imaging of Cardiac Sympathetic Innervation by ^{11}C-*m*HED and PET: From Man to Mouse?

Marilyn P. Law[1,2], Klaus Schäfers[2], Klaus Kopka[1], Stefan Wagner[1], Otmar Schober[1], and Michael Schäfers[2]

[1]*Department of Nuclear Medicine, University Hospital, University of Münster, Münster, Germany; and* [2]*European Institute for Molecular Imaging (EIMI), University of Münster, Münster, Germany*

Dysfunction of the sympathetic nervous system underlies many cardiac diseases and can be assessed by molecular imaging using PET in humans. Small-animal PET should enable noninvasive quantitation of the sympathetic nervous system in mouse models of human disease. For mice, however, the radioactivity needed to give acceptable image quality may be associated with a mass of unlabeled compound sufficient to block the binding of radioligand to its target. The present study assesses the feasibility of using [*N-methyl*-^{11}C]*meta*-hydroxyephedrine (^{11}C-*m*HED) to measure norepinephrine reuptake in humans, to determine cardiac innervation in mice. **Methods:** Anesthetized mice were placed in a small-animal PET scanner. ^{11}C-*m*HED (containing 18% precursor metaraminol) was injected via a tail vein into each animal simultaneously. Fifteen minutes later, animals were injected with saline or metaraminol which competes with *m*HED for norepinephrine reuptake. ^{18}F-FDG was injected at 60 min to identify heart regions. After reconstruction of the list-mode data, radioactivity in myocardial regions was computed using in-house software, and time–activity curves were plotted. **Results:** Hearts were clearly visualized after injection of ^{11}C-*m*HED. Injection of metaraminol at doses less than 50 nmol·kg^{-1} had no effect, whereas doses greater than 100 nmol·kg^{-1} caused a dose-dependent loss of specifically bound radioactivity. **Conclusion:** ^{11}C-*m*HED was successfully used to visualize and assess myocardial innervation in mice. Uptake of ^{11}C-*m*HED is displaceable by the false transmitter metaraminol. The total molar dose of metaraminol and ^{11}C-*m*HED must be considered in the analysis of PET data.

Key Words: ^{11}C-*meta*-hydroxyephedrine; norepinephrine reuptake; sympathetic innervation; cardiac imaging; small-animal PET

J Nucl Med 2010; 51:1269–1276
DOI: 10.2967/jnumed.110.074997

The activity of the sympathetic nervous system (SNS) is increased in heart failure because of an increased sympathetic drive and decreased activity and density of the neuronal norepinephrine reuptake transporter (uptake$_1$). As a consequence, β-adrenoceptors are chronically activated, leading to a downregulation in cardiac β-adrenoceptor density (*1*). Several radioligands are available to investigate the cardiac SNS in patients using PET (*2*). The most widely used clinically are the norepinephrine mimetic ^{11}C-*meta*-hydroxyephedrine (^{11}C-*m*HED) for uptake$_1$ and the nonselective β-adrenoceptor radioligand ^{11}C-CGP 12177 for β-adrenoceptor density. Our group has observed global decreases in both uptake$_1$ and β-adrenoceptor density in nonischemic arrhythmogenic cardiomyopathies (*3–5*), whereas enhanced reuptake occurred without a change in β-adrenoceptor density in Brugada syndrome (*6*).

The development of small-animal PET scanners with both a high resolution and a high sensitivity offers the possibility of studying the progression of disease processes in rat and mouse models of human heart failure. In contrast to the wide use of ^{18}F-FDG to assess myocardial metabolism (*7*), however, there are few published PET studies of myocardial SNS in rodents, although small-animal PET has been used in rats to assess myocardial sympathetic neuronal activity (*8*) and to evaluate radioligands for β_1-adrenoceptors (*9*).

The use of PET to image molecular targets such as transporters or receptors in small animals imposes challenges not apparent in studies using metabolic tracers such as ^{18}F-FDG, which can be given at the high concentrations needed to achieve good images. Scanner design aims to optimize both resolution and sensitivity, but in dedicated animal scanners resolution is often pursued at the expense of sensitivity so that high doses of radioactivity or long acquisition times are required. With current radiopharmaceutical production methods, high doses of radioactivity are associated with a significant amount of unlabeled compound, which may compromise the specific binding of the radioligand (*10*).

The quadHIDAC small-animal PET scanner (Oxford Positron Systems) (*11*) has a good spatial resolution and high sensitivity (*12,13*). Good-quality images of the mouse heart are achievable using less than 5 MBq of ^{18}F-FDG—which, at a specific activity of 30 GBq·μmol^{-1}, is equivalent to 0.17 nmol, giving 5.6 nmol·kg^{-1} for a 30-g mouse.

Received Jan. 19, 2010; revision accepted Mar. 24, 2010.
For correspondence or reprints contact: Marilyn P. Law, European Institute for Molecular Imaging, University of Münster, Mendelstrasse 11, D-48149 Münster, Germany.
E-mail: mplaw@uni-muenster.de

At this dose, the specific binding of a high-affinity radioligand, such as (*S*)-^{11}C-CGP 12177 (in vivo K_D ~1 nmol·kg^{-1} (*14*)), is not detectable, whereas specific uptake of radiotracers with moderate affinity, for example, ^{11}C-*m*HED (in vivo K_D ~100 nmol·kg^{-1} (*15*)), is evident.

The aim of the present work was to test the feasibility of assessing myocardial uptake$_1$ in mice using ^{11}C-*m*HED with the high-resolution quadHIDAC small-animal PET scanner and to develop a quantitative measure of uptake$_1$. With the current radiosynthesis of ^{11}C-*m*HED, a small amount of the precursor metaraminol is also present in the dispensed ^{11}C-*m*HED. Metaraminol is a norepinephrine mimetic with an in vivo K_i (~120 nmol·kg^{-1}) in rat myocardium that is similar to that for *m*HED (*15*). Therefore, the effect of metaraminol on myocardial ^{11}C-*m*HED radioactivity was investigated.

MATERIALS AND METHODS

Radiochemistry

^{11}C-*m*HED was synthesized by direct *N*-methylation of metaraminol with no-carrier-added ^{11}C-iodomethane (*16*). Specific radioactivities at the end of synthesis were 10–30 GBq·μmol^{-1}. Radiochemical purities were 95% ± 5%. For 12 preparations, the mean concentrations of *m*HED and metaraminol were 9 and 2 μM, respectively.

Pharmaceuticals

Metaraminol bitartrate was purchased from Sigma Aldrich Chemie GmbH. It was dissolved in saline at concentrations of 50 nmol·mL^{-1} to 10 μmol·mL^{-1} for injection.

Animals

Studies were approved by the federal animal rights committee and were performed in accordance with institutional guidelines for health and care of experimental animals.

Male C57Bl6 mice (25–35 g) were anesthetized by inhalation (isoflurane; 2%; oxygen, 0.5 L·min^{-1}) for insertion of catheters into a lateral tail vein and, in some animals, the ventral tail artery. Animals were allowed to recover for 1−2 h under light restraint before being reanesthetized for PET. Ex vivo biodistribution studies were performed in conscious animals.

PET

PET was performed using a submillimeter-resolution (0.7 mm in full width at half maximum) dedicated small-animal scanner (32-module quadHIDAC), which uses wire-chamber detectors and offers uniform spatial resolution over a large cylindric field (diameter, 165 mm; axial length, 280 mm) (*11–13*).

Two or 4 anesthetized mice (isoflurane, 2%; oxygen, 0.5 L·min^{-1} per mouse) with tail vein catheters were positioned in the scanner lying on their abdomens on a heating pad to maintain body temperature during the scan. Injections were performed via the tail vein catheters using injection loops made from fine-bore polythene tubing and flushed with saline by an infusion pump.

To assess myocardial uptake, ^{11}C-*m*HED (3−7 MBq in 100 μL per mouse; *m*HED, 2−90 nmol·kg^{-1}; metaraminol, 1–24 nmol·kg^{-1}) was injected simultaneously into each mouse at 30 s after the start of data acquisition (total injection volume, including saline flush, 200 μL). To assess displacement of ^{11}C-*m*HED, one mouse was given 50 μL of saline, and the other mouse (or the other 3 mice in the 4-mouse groups) was given 50 μL of metaraminol (0.04−40 μmol·kg^{-1}) at 15 min after injection of ^{11}C-*m*HED (total injection volume, 150 μL). List-mode data were acquired for 60 min. To confirm the location of the heart, ^{18}F-FDG (4–8 MBq in 50 μL per mouse; total injection volume, 150 μL) was injected via the tail vein at 5−10 min after completion of the ^{11}C-*m*HED scan, and data were acquired for 30 min.

A similar procedure was used to assess competition between ^{11}C-*m*HED and metaraminol. Unlabeled metaraminol was added to dispensed ^{11}C-*m*HED at concentrations to give doses of 0.1−1 μmol·kg^{-1}. The prepared ^{11}C-*m*HED (100 μL) was injected at 30 s after scan start, and list-mode data were acquired for 60 min. ^{18}F-FDG was then injected to confirm the location of the heart.

Data Analysis

List-mode data were reconstructed into images with a voxel size of 0.4 × 0.4 × 0.4 mm^3 in time frames of 10 s, 20 s, 1 min, 10 min, or 20 min for ^{11}C-*m*HED and 15 min for ^{18}F-FDG, using an iterative reconstruction algorithm (*17*). PET images were analyzed using in-house software programs in MATLAB (The MathWorks Co.) and C programming languages (*13*).

To assess the total radioactivity in each animal, a cube encompassing the body, excluding the tail and paws, was drawn on the reconstructed ^{18}F-FDG image (time frame, 15–30 min). The parameters defining this cube were saved and used to compute the whole-body radioactivities (counts per second [cps]·mL^{-1}) for each time frame of the ^{11}C-*m*HED scan.

The parameters required to create images of each heart and compute time–activity curves were also defined using the ^{18}F-FDG scan (time frame, 15–30 min). The reconstructed volume was divided into 2 or 4 subimages, each showing 1 mouse. From the subimages, coronal images (64 × 64 × 64 pixels) encompassing the heart were made, and regions of interest were drawn manually for myocardium (left ventricular wall and septum) and blood (left ventricular chamber). The parameters were saved and used to create heart images (time frames, 5−15 and 40−60 min) and decay-corrected time–activity curves (cps·mL^{-1} vs. mid-frame time, for each 10-s, 20-s, or 1-min time frame after injection) for the ^{11}C-*m*HED scan.

Ex Vivo Studies

^{11}C-*m*HED (*m*HED, 2 or 47 nmol·kg^{-1}; metaraminol, 1 or 3 nmol·kg^{-1}) mixed with increasing concentrations of added metaraminol (0.1−10 μmol·g^{-1}) was injected as a bolus (100 μL) via the tail vein. Aliquots of each injectate were diluted in ethanol–saline and measured to determine the radioactivity injected into each mouse. Mice were sacrificed by intravenous injection of sodium pentobarbitone (Narcoren; Merial GmbH) at 200 mg·(kg of body weight)$^{-1}$ at 30 min after injection. Blood was taken by cardiac puncture and tissues rapidly removed, blotted dry using filter paper, and weighed. Radioactivity was measured using an automated γ-counter (Wallac Wizard 3; Perkin Elmer Life Sciences). To correct for differences in animal body weight and injected dose, results were expressed as an uptake index (*15*), defined as:

$$\text{Uptake index} = \frac{\text{Tissue radioactivity (cpm)/tissue wet weight (g)}}{\text{Radioactivity injected (cpm)/body weight (g)}}.$$

To assess clearance of ^{11}C-*m*HED radioactivity from the blood, sequential blood samples were collected by dripping blood from a tail artery catheter into a multiwell plate (10-s collection times).

Samples were weighed and radioactivity measured using the automated γ-counter. Radioactivity was expressed as cpm·g^{-1}.

RESULTS

PET Scans

^{11}C-*m*HED in combination with high-resolution small-animal PET resulted in images of the SNS in mice that were comparable to those achieved in humans with respect to resolution and contrast. The heart was no longer visible after the injection of metaraminol, but its position was confirmed by ^{18}F-FDG (Fig. 1).

Myocardial Uptake of ^{11}C-*m*HED

Myocardial images for the mice in Figure 1 are shown in Figures 2A−2F. The late ^{11}C-*m*HED images (Figs. 2B and 2E) indicated that the apex and part of the septum included spillover from the liver. Therefore, to construct time–activity curves for the myocardium, regions of interest were traced manually round the left ventricular wall and septum (omitting the apical region) on the ^{18}F-FDG image and confirmed on the ^{11}C-*m*HED images. Results for the left ventricular wall are shown in Figure 2G. The data for mouse 1 were fitted by a biexponential function of the form $y = ae^{-bx} + ce^{-dx}$. The data for mouse 2 were fitted by a biexponential function before injection of metaraminol and by a single exponential function of the form $y = ae^{-bx} + y_0$ after metaraminol administration. Myocardial radioactivity was detected immediately after injection and reached a maximum during the first minute. The early phase (<5 min) of rapid loss from the left ventricular wall (blood pool) was followed by a slow loss of myocardial radioactivity. The injection of unlabeled metaraminol, but not saline, caused a rapid loss of myocardial radioactivity. It also caused a rapid loss of activity from the ventricular space, an observation consistent with a high spillover from the myocardium (data not shown).

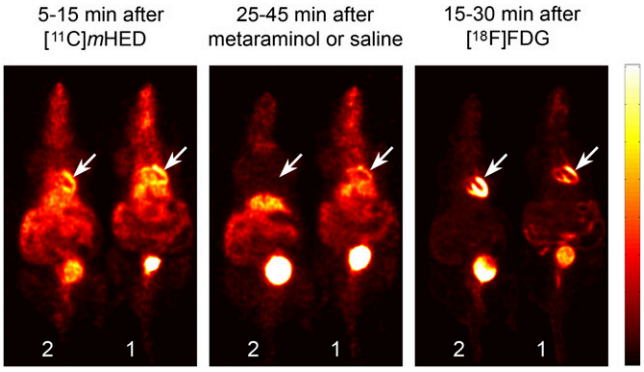

FIGURE 1. Distribution of radioactivity after simultaneous intravenous injection of ^{11}C-*m*HED (3.6 MBq, 22.8 nmol·kg^{-1}) into 2 mice. Fifteen minutes after ^{11}C-*m*HED, mouse 2 received metaraminol (40 μmol·kg^{-1} intravenously) and mouse 1 saline. Both mice received ^{18}F-FDG (5 MBq) after ^{11}C-*m*HED scan. Arrows indicate hearts.

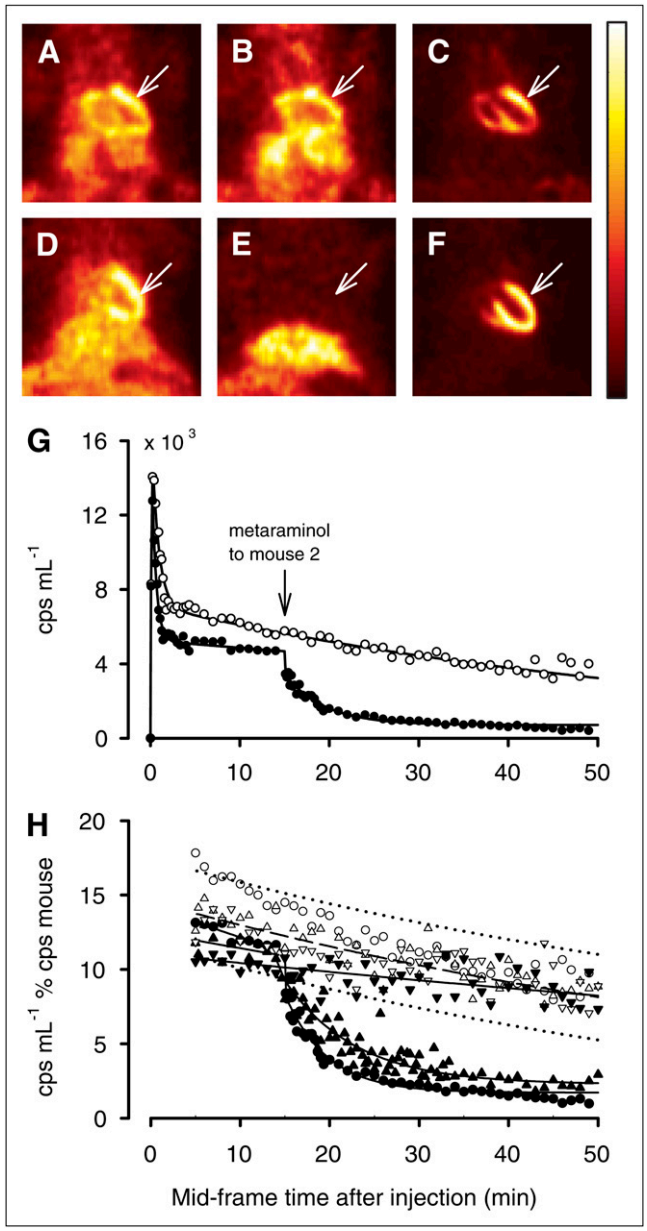

FIGURE 2. Uptake of radioactivity in mouse heart after intravenous injection of ^{11}C-*m*HED. (A–F) Images of thoraces of the 2 mice in Figure 1 (scan 1): mouse 1 (A−C); mouse 2 (D−F). Both hearts (arrows) were visualized at 5−15 min after ^{11}C-*m*HED (A and D). Heart was still visible at 25–45 min after saline (B) but not after metaraminol (E) administration. ^{18}F-FDG confirmed heart positions (C and F). (G) Time–activity curves for left ventricular wall (○, mouse 1; ●, mouse 2). (H) Normalized time–activity curves for scan 1, with results for 2 other scans (scans 2 and 3). In each scan, one mouse was injected with saline at 15 min after ^{11}C-*m*HED (○, scan 1; Δ, scan 2; ▽, scan 3) and the other with metaraminol (● = 40 μmol·kg^{-1}, scan 1; ▲ = 208 nmol·kg^{-1}, scan 2; ▼ = 100 nmol·kg^{-1}, scan 3). Broken line shows single exponential fit to control data (7 mice) and dotted lines 95% inclusion limits. Solid line shows fits to metaraminol displacement for each dose.

There was a discrepancy between blood time–activity curves derived from PET images and those assessed by continuous arterial blood sampling (Supplemental Fig. 1; supplemental materials are available online only at http://jnm.snmjournals.org). In the absence of corrections for scatter and spillover (Supplemental Fig. 2), it is not possible to obtain an input function by drawing a region in the left ventricle.

Displacement of ^{11}C-*m*HED by Metaraminol

Because there is no noninvasive method for obtaining an input function, myocardial radioactivity ($cps \cdot mL^{-1}{}_{myocardium}$) was normalized to the total radioactivity in the mouse (cps_{mouse}) for each time frame.

$$cps \cdot mL^{-1}\% \, cps_{mouse} = 100\left(cps \cdot mL^{-1}\right)_{myocardium}/(cps_{mouse}). \quad \text{Eq. 1}$$

Figure 2H shows normalized myocardial uptake for the 2 mice in Figures 2A−2G, with the results for 2 other pairs of mice. For each pair, one mouse was injected with saline (intravenously) at 15 min after ^{11}C-*m*HED (control mouse) and the other mouse with metaraminol (test mouse). For clarity of illustration, data points for minute time frames are shown. Metaraminol at 40 μmol·kg^{-1} or 208 nmol·kg^{-1} caused rapid loss of myocardial ^{11}C-*m*HED, but 100 nmol·kg^{-1} had no significant effect.

Injecting metaraminol at high doses (>500 nmol·kg^{-1}) after ^{11}C-*m*HED caused a rapid loss of myocardial radioactivity, approximately 70% being displaced during the first 5 min. Therefore, to assess the effect of metaraminol, 10- and 20-s frames were reconstructed for the first 10 min after displacement. Normalized time–activity curves were computed, omitting the first 10-s frame, during which metaraminol was being injected, and using 10-s, 20-s, and subsequent minute time frames.

Normalized time–activity curves for control mice were fitted by a single exponential function

$$y = ae^{-bx}, \quad \text{Eq. 2}$$

where y is myocardial activity, and x is the time after injection of ^{11}C-*m*HED.

Normalized time–activity curves for test mice were fitted by a single exponential function (Eq. 2) before injection of metaraminol (5–15 min after ^{11}C-*m*HED) and by a single exponential function with a nondisplaceable background B (Eq. 3) after metaraminol administration (15–50 min after ^{11}C-*m*HED).

$$y = ae^{-bx} + B. \quad \text{Eq. 3}$$

To compare individual control mice, the washout of ^{11}C-*m*HED radioactivity was expressed as the rate constant b in Equation 2 for 5–50 min after injection and area under the curve (AUC) for 5–50 min ($AUC_{5–50\ min}$). Values for slope b ranged from 0.004 to 0.017 (mean, 0.0122; SE, 0.0015; $n = 7$), and there was no correlation between the nanomolar dose of norepinephrine mimetics (*m*HED plus metaraminol) injected (<2–77 nmol·kg^{-1}) and slope b. Values for the $AUC_{5–50\ min}$ (mean, 480; SE, 19; $n = 7$) were not related to injected doses below 35 nmol·kg^{-1}, but 2 animals that received doses of 62 and 77 nmol·kg^{-1} showed low values (250 and 212, respectively).

For comparison with mice that received displacement metaraminol, data for control mice before or after injection of saline (5–15 min or 15–45 min after ^{11}C-*m*HED) were also fitted by a single exponential function (Eq. 2). Estimates of rate b and AUCs (AUC for 5–15 min, $AUC_{5–50\ min}$, and AUC for 15–50 min) were not significantly different from those for the fits to data for 5–50 min.

The early washouts of myocardial radioactivity (5–15 min after ^{11}C-*m*HED) for control (0.013 ± 0.002 min^{-1}, $n = 9$) or test (0.014 ± 0.003 min^{-1}, $n = 12$) mice were not significantly different ($P = 0.72$, Student t test; $P = 0.65$, paired t test).

Relationships between rate b for 15–50 min after ^{11}C-*m*HED or AUC for 15–45 min ($AUC_{15–45\ min}$) and metaraminol dose are shown in Figure 3. Results for control mice are plotted against metaraminol (dispensed) injected with ^{11}C-*m*HED (Figs. 3A and 3C), and those for test mice are plotted against metaraminol (displacement) injected at 15 min after ^{11}C-*m*HED (Figs. 3B and 3D). The sum of *m*HED (2–69 nmol·kg^{-1}) and dispensed metaraminol (1–24 nmol·kg^{-1}) ranged from 3 to 104 nmol·kg^{-1}. In some cases, therefore, the amount of norepinephrine mimetic (*m*HED plus metaraminol) injected at time 0 was greater than the displacement dose of metaraminol given at 15 min (40 nmol·kg^{-1} to 40 μmol·kg^{-1}).

For control mice, the rate of loss (0.0092 ± 0.0005 min^{-1}) did not depend on the dose of mimetic injected (Fig. 3A), but displacement metaraminol at doses greater than 100 nmol·kg^{-1} caused rapid loss (Fig. 3B). The displacement data were fitted to an equation of the form

$$y = (rate_{max} \cdot x)/(K_{dis} + x), \quad \text{Eq. 4}$$

where $rate_{max}$ is the maximum rate of radioactivity loss, x is the displacement metaraminol dose, and K_{dis} is the half-saturation dose. Nonlinear least-squares estimates of the parameters calculated using all data points in Figure 3B were $rate_{max} = 0.33 \pm 0.4$ min^{-1} and $K_{dis} = 296 \pm 138$ nmol·kg^{-1} ($R = 0.87$). Omitting the 2 mice with the highest dose of mimetic at time 0 and the mouse with no quality control information did not significantly change the fit.

The $AUC_{15–45\ min}$ for control mice (Fig. 3C) indicates that metaraminol doses less than 25 nmol·kg^{-1} injected with *m*HED doses less than 60 nmol·kg^{-1} have no effect on myocardial uptake of radioactivity. Values for test mice, plotted against displacement metaraminol (Fig. 4D), howed a sharp decrease above approximately 50 nmol·kg^{-1}. Mice in 1 experiment received exceptionally high doses of ^{11}C-*m*HED (68–93 nmol·kg^{-1}). The AUCs for these mice were significantly lower than for mice that

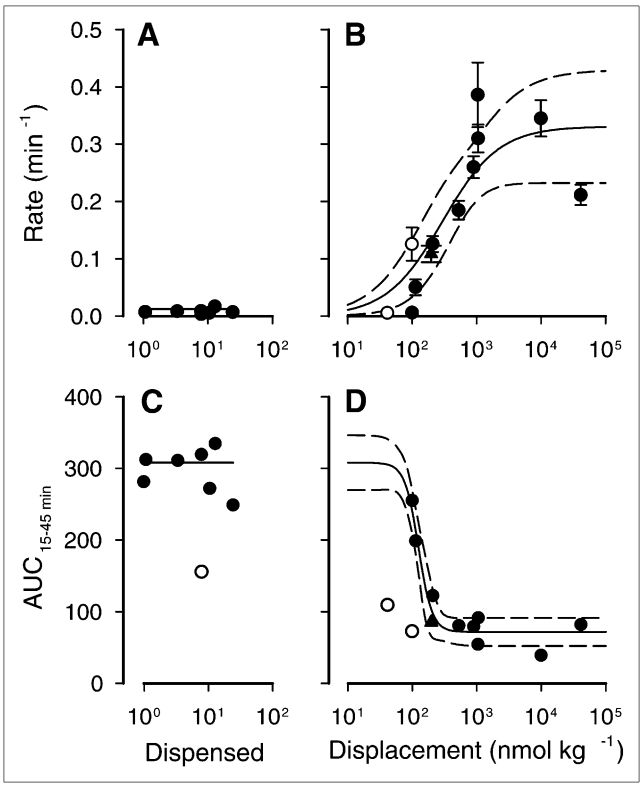

FIGURE 3. Displacement of ^{11}C-*m*HED radioactivity from myocardium by intravenous injection of metaraminol. ^{11}C-*m*HED injected at time 0 (●, 2–60 nmol·kg^{-1}; ○, 70–90 nmol·kg^{-1}) was associated with metaraminol (dispensed) (1–24 nmol·kg^{-1}). No quality control was available for 1 scan of 2 mice (▲). (A and C) Data for control mice as function of dispensed metaraminol. (B and D) Data for test mice as function of metaraminol (displacement) injected 15 min after ^{11}C-*m*HED. (B) Solid line shows nonlinear least-squares fit to all data points. (D) Solid line shows nonlinear least-squares fit to data points for which ^{11}C-*m*HED is ≤60 nmol·kg^{-1}. Broken lines show 95% confidence limits.

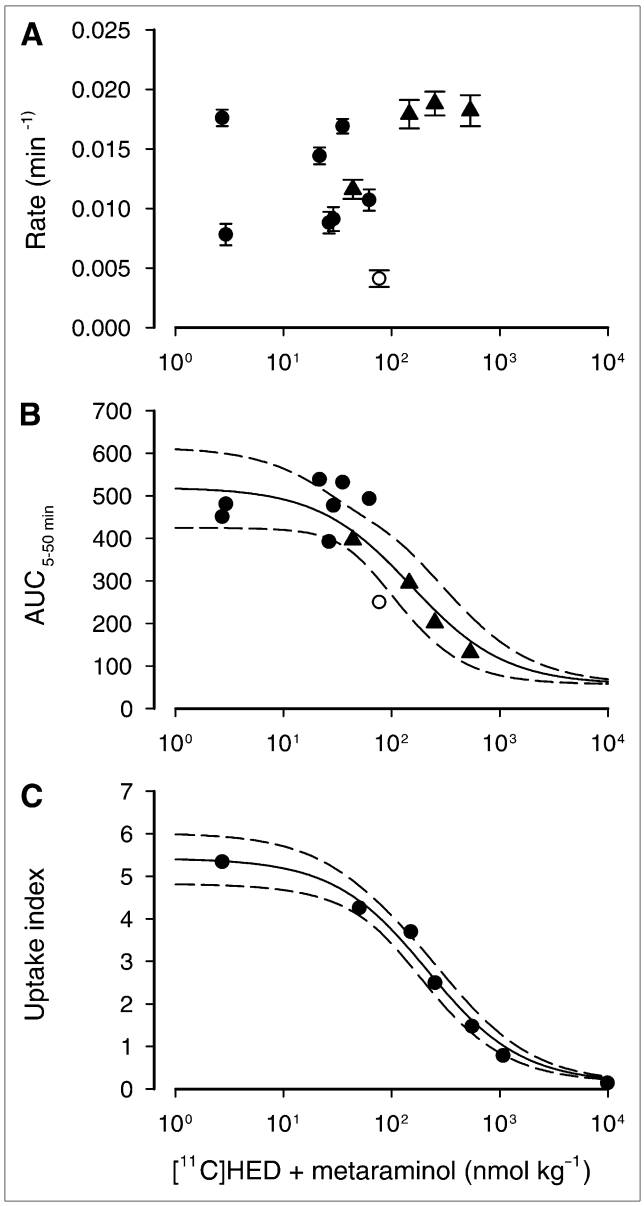

FIGURE 4. Dose–effect relationships for myocardial uptake of ^{11}C-*m*HED radioactivity. (A and B) In vivo PET. Saline or increasing doses of metaraminol (100, 200, or 500 nmol·kg^{-1}) were coinjected with fixed amounts of dispensed ^{11}C-*m*HED (44 nmol·kg^{-1}) and metaraminol (0.8 nmol·kg^{-1}) (▲). Control mice (from Fig. 3) were injected with ^{11}C-*m*HED (●, 2–60 nmol·kg^{-1}; ○, 70–90 nmol·kg^{-1}) and metaraminol at less than 24 nmol·kg^{-1}. (A) Rates of loss of radioactivity. (B) AUCs. (C) Ex vivo dissection. Saline or increasing doses of metaraminol were coinjected with fixed amounts of dispensed ^{11}C-*m*HED (2–47 nmol·kg^{-1}) and metaraminol (1–3 nmol·kg^{-1}) into conscious mice. Radioactivity at 30 min after injection expressed as uptake index is shown. Solid lines represent nonlinear least-squares fits to data points and broken lines 95% confidence limits.

received similar doses of metaraminol but lower doses of ^{11}C-*m*HED and were omitted from further analysis. AUCs for mice that received displacement metaraminol were fitted by a 4-parameter logistic equation:

$$y = \mathrm{D} + (\mathrm{A} - \mathrm{D}) / \left(1 + \left[x / \left(10^{\log \mathrm{C}}\right)^{\mathrm{B}}\right]\right), \qquad \text{Eq. 5}$$

where y is the AUC; x is the displacement metaraminol dose (nmol·kg^{-1}); C is the metaraminol dose for half-maximal displacement; and A, B, and D are parameters giving a half-maximal dose of 124 nmol·kg^{-1}.

Effect of Injected Dose on Myocardial Uptake of ^{11}C-*m*HED

Studies in rats have shown that myocardial uptake of ^{11}C-*m*HED is reduced if the combined dose of *m*HED and metaraminol is greater than approximately 20 nmol·kg^{-1} and the half-saturation dose is approximately 100 nmol·kg^{-1} (*15*). The present displacement studies suggest that these doses are higher in mice (>100 nmol·kg^{-1}). To further investigate this effect, saline or increasing doses of metaraminol were coinjected with a fixed amount of dispensed

^{11}C-*m*HED and metaraminol. Time–activity curves were constructed using minute time frames, and the rates or AUCs (computed using Eq. 2) were plotted against the combined dose of ^{11}C-*m*HED and metaraminol (Figs. 4A and 4B). Data for all control mice in Figure 3 are plotted for comparison. There was no correlation between rate of loss of ^{11}C-*m*HED radioactivity and injected dose. The AUC, however, decreased with doses above 100 nmol·kg^{-1}. Assuming ^{11}C-*m*HED, *m*HED, and metaraminol have similar affinities and binding potentials (β_{max}/K_d) for uptake$_1$ transporters (*15*), the data were fitted to:

$$AUC = B+(\beta_{max}/K)(1/[1+C/K]), \quad \text{Eq. 6}$$

where C is the injected dose (*m*HED + metaraminol), B is the nondisplaceable background, β_{max} is the maximum uptake, and K is the half-saturation constant (*15*) (≈ half-saturation dose). B was set at 87.09 (B in Eq. 3 for displacement by 10 and 40 μmol·kg^{-1} metaraminol multiplied by 45 min), giving a K value of 132 ± 59 nmol·kg^{-1} (R = 0.86).

Ex vivo dissection studies gave comparable results (Fig. 4C). ^{11}C-*m*HED mixed with increasing concentrations of added metaraminol was injected as a bolus via the tail vein into conscious mice. The data were fitted to:

$$\text{Uptake index} = B+(\beta_{max}/K)(1/[1+C/K]), \quad \text{Eq. 7}$$

where C is the injected dose (*m*HED + metaraminol), B is the nondisplaceable background, β_{max} is the maximum uptake, and K is the half-saturation constant. B was fixed to 0.14, the uptake index at 10 μmol·kg^{-1}, giving a K value of 215 ± 32 nmol·kg^1 (R = 0.99).

Dose–effect relationships are summarized in Table 1.

DISCUSSION

The present study demonstrates that myocardial sympathetic innervation can be visualized in mice using the established tracer ^{11}C-*m*HED with the high-resolution quadHIDAC small-animal PET scanner. Displaceable specific uptake can be demonstrated and pharmacokinetic parameters measured. This opens an exciting window of opportunity for future work on sympathetic innervation in mouse models of cardiovascular diseases.

The unique advantage of the quadHIDAC scanner is that it offers a high sensitivity and high spatial resolution, which is constant over a large field of view (*13*). Consequently, several mice may be scanned at the same time, allowing the effects of pharmacologic interventions to be compared using the same radiochemical preparation. This is especially valuable for neuroreceptor systems in which specific uptake of a radioligand is reduced as the amount of unlabeled ligand increases (i.e., as specific activity decreases).

Notwithstanding the limitations imposed by the lack of absolute quantitation in small-animal PET scanners, tracer modeling may give estimates of relevant physiologic parameters. Essentially two methods have been applied to assess myocardial innervation using ^{11}C-*m*HED in patient studies, both of which require an arterial input function based on serial measurements of blood activity, either by blood sampling or by selecting volumes of interest in a heart chamber (*4,18*). Serial blood sampling in mice, however, necessitates catheterization of major blood vessels, which is not practical if serial scans are to be obtained to assess the development of disease or therapeutic efficacy. Determining the input function from PET images is an attractive alternative, but spillover from myocardium to the ventricles (blood pool) makes this approach inappropriate for mice. The only option in mice, therefore, was to use a semiquantitative index as previously used in humans (*19*). Time–activity curves were constructed using normalized myocardial radioactivity (cps·mL^{-1}% cps_{mouse}). Both washout of ^{11}C-*m*HED radioactivity and AUCs were calculated.

The PET scans of mice showed changes in myocardial radioactivity (Fig. 2) that were comparable to those after a bolus injection of ^{11}C-*m*HED in rats, assessed by ex vivo dissection (*15,20*) or PET (*8*). An early increase in activity was followed by a phase of rapid decrease (from 20 s to 2 min) reflecting rapid loss from vascular space and then by a phase of slow loss from the myocardium. Metabolite analysis was not performed in this study. In rats, however, although radioactive metabolites were detected in plasma, only parent ^{11}C-*m*HED was detected in the myocardium (*15,20*). The data for 5–50 min (Fig. 2) were fitted by a monoexponential function on the basis that loss of ^{11}C-*m*HED from the nerve terminals is a process that follows first-order kinetics. The rate of loss ranged from 0.04 to 0.176 min^{-1}; there was no relationship between rate of loss and injected nanomolar dose. Values for areas under the time–activity curves ($AUC_{5–50\ min}$) ranged from 400 to 540 for injected doses less than 60 nmol·kg^{-1}.

A bolus injection of unlabeled metaraminol at 15 min after injection of ^{11}C-*m*HED displaced myocardial radioactivity (Fig. 2), as has been observed ex vivo in rats (*15*). To assess the effect of metaraminol dose, the time–activity curves after injection of metaraminol were fitted by a monoexponential function with a background. The rate of loss increased from 0.1 to 1 μmol·kg^{-1} with metaraminol dose and was fitted by Michaelis–Menten kinetics, assuming that displacement by metaraminol is a pseudobimolecular reaction. An alternative measure of the effect of metaraminol was to calculate AUCs after injection of saline or metaraminol ($AUC_{15–45\ min}$, Fig. 3). This parameter showed a sharp decrease as metaraminol dose was increased above approximately 50 nmol·kg^{-1}.

The study in which metaraminol was coinjected with ^{11}C-*m*HED (Fig. 4) indicated that the rate of loss of myo-

TABLE 1. Myocardial Retention of ^{11}C-*m*HED

Study	Equation	Regression coefficient *R*	Dose for half-maximum effect (nmol·kg^{-1})
Displacement by metaraminol (PET)	4	0.866	296
	5	0.978	124
Coinjection of metaraminol + ^{11}C-*m*HED (PET)	6	0.858	132 ± 59
Coinjection of metaraminol + ^{11}C-*m*HED (dissection)	7	0.993	215 ± 32

cardial ^{11}C-*m*HED did not depend on injected dose, whereas the $AUC_{5–50\ min}$ showed a clear dependence due to a reduced initial uptake. Comparable results were obtained by ex vivo dissection studies (Fig. 4).

The rate of displacement of ^{11}C-*m*HED by metaraminol was the parameter least sensitive to metaraminol dose; the dose for half maximum was approximately 300 nmol·kg^{-1} (Table 1). The competition studies indicated that although the rate of loss of ^{11}C-*m*HED between 5 and 50 min after injection did not depend on injected dose, the AUC decreased as the total dose of mimetics (^{11}C-*m*HED + *m*HED + metaraminol) increased; the half-saturation constant K was 132 ± 59 nmol·kg^{-1}. A similar relationship between uptake index assessed by ex vivo dissection studies and total dose was observed. In this case, the half-saturation constant K was higher (215 ± 32 nmol·kg^{-1}) but not significantly so. The data presented in Figures 3 and 4 indicate that myocardial uptake of ^{11}C-*m*HED in mice decreases if the total injected dose of *m*HED and metaraminol is greater than approximately 50 nmol·kg^{-1}. This dose, however, may be lower in mouse models of heart disease because the kinetics of uptake and retention of ^{11}C-*m*HED depend on the number of neuronal noradrenaline transporters in the myocardium and on their intrinsic activity. A decrease in the number of transporters without a change in their activity will reduce myocardial uptake of ^{11}C-*m*HED (AUC) but not the half-saturation constant K. A decrease in transporter activity, however, may reduce K. In addition, an increase in endogenous norepinephrine, as is observed in many heart diseases, may reduce the apparent K for injected mimetics.

CONCLUSION

The reuptake of norepinephrine ($uptake_1$) by myocardial sympathetic nerve endings can be successfully visualized in the mouse using ^{11}C-*m*HED with the quadHIDAC small-animal PET scanner, opening exciting perspectives toward future preclinical studies in mouse models. A semiquantitative index can be used to compare $uptake_1$ in individual mice and gain information about pharmacokinetic parameters. Myocardial uptake of ^{11}C-*m*HED is dependent on the nanomolar dose of both *m*HED and metaraminol, the synthesis precursor; a total mimetic dose greater than approximately 50 nmol·kg^{-1} results in a decrease in myocardial uptake. Consequently, it is essential to ensure that the doses of ^{11}C-*m*HED plus any metaraminol used with PET to study $uptake_1$ in mice are below approximately 50 nmol·kg^{-1}.

ACKNOWLEDGMENTS

We thank Christine Bätza, Irmgard Hoppe, Anne Kanzog, Sandra Schröer, Daniel Burkert, and Sven Fatum for excellent technical assistance. This work was supported by the Deutsche Forschungsgemeinschaft, SFB 656 (projects A5, B2, B3, and Z5), by the Interdisciplinary Center for Clinical Research (IZKF core unit SmAP), Münster, Germany, and by the EU-FP6 project Diagnostic Molecular Imaging (DiMI) (WP 11.1), LSHB-CT-2005-512146.

REFERENCES

1. Brodde OE, Leinewever K. Autonomic receptor systems in the failing and aging human heart: similarities and differences. *Eur J Pharmacol.* 2004;500:167–176.
2. Lautamäki R, Tipre D, Bengel FM. Cardiac sympathetic neuronal imaging using PET. *Eur J Nucl Med Mol Imaging.* 2007;34:S74–S85.
3. Schäfers M, Dutka D, Rhodes CG, et al. Myocardial presynaptic and postsynaptic autonomic dysfunction in hypertrophic cardiomyopathy. *Circ Res.* 1998;82:57–62.
4. Schäfers M, Lerch H, Wichter T, et al. Cardiac sympathetic innervation in patients with idiopathic right ventricular outflow tract tachycardia. *J Am Coll Cardiol.* 1998;32:181–186.
5. Wichter T, Schäfers M, Rhodes CG, et al. Abnormalities of cardiac sympathetic innervation in arrhythmogenic right ventricular cardiomyopathy: quantitative assessment of presynaptic norepinephrine reuptake and postsynaptic β-adrenergic receptor density with positron emission tomography. *Circulation.* 2000;101:1552–1558.
6. Kies P, Wichter T, Schäfers M, et al. Abnormal myocardial presynaptic norepinephrine recycling in patients with the Brugada syndrome. *Circulation.* 2004;110:3017–3022.
7. Schelbert HR, Inubushi M, Ross RS. PET imaging in small animals. *J Nucl Cardiol.* 2003;10:513–520.
8. Tipre DN, Fox JJ, Holt DP, et al. *In vivo* PET imaging of cardiac presynaptic sympathoneuronal mechanisms in the rat. *J Nucl Med.* 2008;49:1189–1195.
9. Law MP, Wagner S, Kopka K, Pike VW, Schober O, Schäfers M. Are [*O*-*methyl*-^{11}C]derivatives of ICI 89,406 β_1-adrenoceptor selective radioligands suitable for PET? *Eur J Nucl Med Mol Imaging.* 2008;35:174–185.
10. Hume SP, Gunn RN, Jones T. Pharmacological constraints associated with positron emission tomographic scanning of small laboratory animals. *Eur J Nucl Med.* 1988;25:173–176.
11. Jeavons AP, Chandler RA, Dettmar CAR. A 3D HIDAC-PET camera with sub-millimetre resolution for imaging small animals. *IEEE Trans Nucl Sci.* 1999;46:468–473.
12. Missimer J, Madi Z, Honer M, Keller C, Schubiger A, Ametamey SM. Performance evaluation of the 16-module quad-HIDAC small animal PET camera. *Phys Med Biol.* 2004;49:2069–2081.
13. Schäfers KP, Reader AJ, Kriens M, Knoess C, Schober O, Schäfers M. Performance Evaluation of the 32-module quadHIDAC small animal PET scanner. *J Nucl Med.* 2005;46:996–1004.
14. Law MP. Demonstration of the suitability of CGP 12177 for *in vivo* studies of β-adrenoceptors. *Br J Pharmacol.* 1993;109:1101–1109.

15. Law MP, Osman S, Davenport RJ, Cunningham VJ, Pike VW, Camici PG. Biodistribution and metabolism of [*N-methyl*-^{11}C]-*m*-hydroxyephedrine in the rat. *Nucl Med Biol.* 1997;24:417–424.
16. Rosenspire KC, Haka MS, vanDort ME, et al. Synthesis and preliminary evaluation of carbon-11-meta-hydroxyepehdrine: a false transmitter agent for heart neuronal imaging. *J Nucl Med.* 1990;31:1328–1334.
17. Reader AJ, Ally S, Bakatselos F, et al. One-pass list-mode EM algorithm for high resolution 3D PET image reconstruction into large arrays. *IEEE Trans Nucl Sci.* 2002;49:693–699.
18. Münch G, Nguyen N, Nekolla BS, et al. Evaluation of sympathetic nerve terminals with [^{11}C]epinephrine and [^{11}C]hydroxyephedrine and positron emission tomography. *Circulation.* 2000;101:516–523.
19. Malizia AL, Melicher JK, Rhodes CG, et al. Desipramine binding to noradrenaline reuptake sites in cardiac sympathetic neurones in man *in vivo. Eur J Pharmacol.* 2000;391:263–267.
20. Thackeray JT, Beanlands RS, Dasilva JN. Presence of specific ^{11}C-meta-hydroxyephedrine retention in heart, lung, pancreas, and brown adipose tissue. *J Nucl Med.* 2007;48:1733–1740.